Inelastic neutron scattering and frequency-domain magnetic resonance studies of $S=4$ and $S=12$ Mn_6 single-molecule magnets

O. Pieper,[1,2,*] T. Guidi,[3,1,†] S. Carretta,[4,5] J. van Slageren,[6,7] F. El Hallak,[6] B. Lake,[1,2] P. Santini,[4,5] G. Amoretti,[4,5] H. Mutka,[8] M. Koza,[8] M. Russina,[1] A. Schnegg,[1] C. J. Milios,[9] E. K. Brechin,[9] A. Julià,[10] and J. Tejada[10]

[1]*Helmholtz-Zentrum Berlin für Materialien und Energie (HZB), Hahn-Meitner-Platz 1, 14109 Berlin, Germany*

[2]*Institut für Festkörperphysik, Technische Universität Berlin, Hardenbergstraße 36, 10623 Berlin, Germany*

[3]*ISIS Facility, Rutherford Appleton Laboratory, Chilton, Didcot, Oxon OX11 0QX, United Kingdom*

[4]*Dipartimento di Fisica, Università and Unità CNISM di Parma, I-43100 Parma, Italy*

[5]*National Research Center on nanoStructures and bioSystems at Surfaces (S3), CNR-INFM, 41100 Modena, Italy*

[6]*1. Physikalisches Institut, Universität Stuttgart, D-70550 Stuttgart, Germany*

[7]*School of Chemistry, University of Nottingham, Nottingham NG7 2RD, United Kingdom*

[8]*Institute Laue-Langevin, BP 156, F-38042 Grenoble Cedex, France*

[9]*University of Edinburgh, West Mains Road, Edinburgh EH9 3JJ, United Kingdom*

[10]*Departament de Física Fonamental, Facultat de Física, Universitat de Barcelona, Avinguda Diagonal 647, Planta 4, Edifici nou, 08028 Barcelona, Spain*

(Received 2 March 2010; revised manuscript received 26 April 2010; published 21 May 2010)

We investigate the magnetic properties of three Mn_6 single-molecule magnets by means of inelastic neutron scattering and frequency domain magnetic resonance spectroscopy. The experimental data reveal that small structural distortions of the molecular geometry produce a significant effect on the energy-level diagram and therefore on the magnetic properties of the molecule. We show that the giant spin model completely fails to describe the spin-level structure of the ground spin multiplets. We analyze theoretically the spin Hamiltonian for the low-spin Mn_6 molecule ($S=4$) and we show that the excited S multiplets play a key role in determining the effective energy barrier for the magnetization reversal, in analogy to what was previously found for the two high spin Mn_6 ($S=12$) molecules [S. Carretta *et al.*, Phys. Rev. Lett. **100**, 157203 (2008)].

DOI: 10.1103/PhysRevB.81.174420 PACS number(s): 75.50.Xx, 78.70.Nx, 33.35.+r, 75.60.Jk

I. INTRODUCTION

Single-molecule magnets (SMMs) have been the subject of intense research activity since the first and mostly studied one, $Mn_{12}Ac$, was reported.[1] These metal-organic clusters are usually characterized by a large spin ground state S and an easy-axis anisotropy which determines the zero-field splitting (ZFS) of the S state sublevels. The resulting magnetic bistability makes them interesting for magnetic storage applications due to their potential to shrink the magnetic bit down to the size of one single molecule. Until recently and despite the common efforts of chemists and physicists to find suitable systems that could retain the magnetization for a long time at noncryogenic temperatures, $Mn_{12}Ac$ was the system showing the "highest" blocking temperature (3.5 K) and anisotropy barrier (74.4 K).[2] The relaxation time in the classical regime follows the Arrhenius law: $\tau = \tau_0 \exp(U/k_BT)$ (Ref. 3). According to this, there are two key points that have to be considered for the realization of an ideal SMM. First of all, the anisotropy barrier, given to a first approximation by $U \sim |D|S^2$ (D is the axial anisotropy parameter), has to be sufficiently high. This is to prevent the reversal of the magnetization via a classical thermally activated multistep Orbach process mediated by spin-phonon interactions. This can be achieved by the simultaneous increase in D and S, two variables that are intrinsically linked together.[4] Second, the pre-exponential factor τ_0 in the Arrhenius law has to be large. This factor is dominated by the time necessary to climb the upper states in the energy-level diagram and is proportional to D^{-3} (Refs. 3, 5, and 6). In addition to the classical relaxation mechanism, the quantum tunneling of the magnetization that characterizes the spin dynamics of SMMs, has to be taken into consideration and minimized for magnetic data storage application, since it provides a shortcut for the relaxation of the magnetization.

Therefore, to engineer SMMs able to retain the magnetization for long time it is crucial to control all the different mechanisms that provide a relaxation path for the system. Recently we succeeded in the synthesis of a new class of Mn^{3+}-based clusters that contributed in raising the anisotropy barrier and has served as a good model system to study the factors involved in the relaxation mechanism.[7,8]

This class consists of hexanuclear Mn^{3+} clusters (from now on Mn_6) which, despite the generally similar nuclear structure, display a rich variety of spin ground states and anisotropy energy barriers.[9–14] The six Mn^{3+} ions are arranged in two triangles, with dominant ferromagnetic (FM) exchange interaction between the two triangles and FM or antiferromagnetic (AFM) interactions within the two triangles. It has been found that the nature of the intratriangle exchange interaction can be switched from AFM to FM by substituting the organic ligands bridging the Mn^{3+} ions, leading to a change in the ground state from a low spin ($S=4$) to a high spin ($S=12$).[9] Furthermore, deliberately targeted structural distortions have been successfully used to tune the values of the exchange interactions.[10] The isotropic exchange interactions, and consequently the overall anisotropy barrier,[7] is thus found to be very sensitive to the structural details. This has been also demonstrated using an alternative method for distorting the molecule, that is, by applying external hy

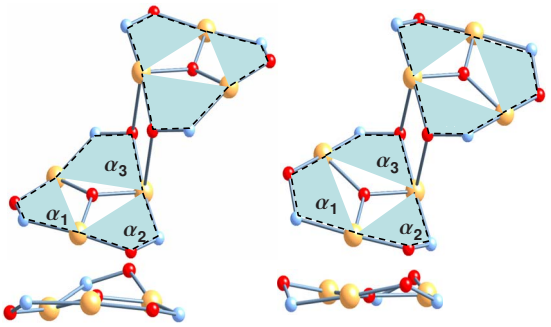

FIG. 1. (Color online) Core of molecules (1) (left) and (3) (right) showing at the bottom the difference in torsion angles (α_1, α_2, and α_3). Color scheme: Mn, large orange circles; O, dark red circles; and N, small light blue circles. H and C ions are omitted for clarity.

drostatic pressure and correlating the structural changes with the magnetic behavior.[15] It is therefore quite important to determine the exchange interactions for different structures to deduce magnetostructural correlations. This information can be then used to engineer new clusters with selectively modified molecular structures that match the optimized conditions for the desired magnetic properties.

We have investigated three members of the family of Mn_6 clusters, with chemical formulas (1) $[Mn_6O_2(sao)_6(O_2CMe)_2(EtOH)_4]\cdot 4EtOH$, (2) $[Mn_6O_2(Et\text{-}sao)_6(O_2CPh)_2(EtOH)_4(H_2O)_2]\cdot 2EtOH$, and (3) $\{Mn_6O_2(Et\text{-}sao)_6[O_2CPh(Me)_2]_2(EtOH)_6\}$.[9,10,16] All molecules display very similar structures consisting of six Mn^{3+} ions ($s=2$) arranged in two staggered triangular units (see Fig. 1) related by an inversion center.

The only major structural difference between the three clusters resides is the steric effect of the organic ligands used in proximity to the transition-metal ions. However, despite having very similar structures, the three molecules have very different magnetic properties. The coupling between the magnetic ions occurs via superexchange pathways involving oxygen and nitrogen ions and is found to be extremely sensitive to intramolecular bond angles and distances. The particular arrangement of the magnetic ions provides exchange couplings lying in the crossover region between AFM and FM. For this reason, even small structural distortions have tremendous impact on the magnetic properties of the system. For example, while the coupling between the two triangles is ferromagnetic for all molecules, the intratriangular coupling changes from antiferromagnetic in (1) to ferromagnetic in (2) and (3) due to a "twisting" of the oximate linkage. This results in a "switching" of the total spin ground state from $S=4$ to $S=12$. Systematic synthesis and studies of various members of the Mn_6 family have revealed that the nature of the coupling is extremely sensitive to the intratriangular Mn-O-N-Mn torsion angles[12,13] (see Fig. 1). There is a critical value for the torsion angle of $30.85° \pm 0.45°$, above which the pairwise exchange interaction switches from antiferromagnetic to ferromagnetic, while a further enhancement of the angle increases the strength of the FM interaction. This effect has been interpreted in terms of the particular arrangement of the manganese d_{z^2} orbitals with respect to the p orbitals of the nitrogen and oxygen ions. A large (small) Mn-O-N-Mn torsion angle results in a small (large) overlap between the magnetic orbitals giving rise to ferromagnetic (antiferromagnetic or weak ferromagnetic) superexchange interactions.[17]

Molecules (2) and (3) have the same spin ground state $S=12$ but very different effective energy barriers [$U_{\text{eff}} \approx 53$ K for (2) and $U_{\text{eff}} \approx 86.4$ K for (3)]. This difference was found to be closely related to the exchange interactions.[7]

In order to understand this rich variety of behaviors, we performed a detailed spectroscopic characterization of the three molecules using inelastic neutron scattering (INS) and frequency domain magnetic resonance (FDMR). FDMR is only sensitive to transitions with a predominantly intramultiplet character, according to the selection rules $\Delta S=0$, $\Delta M_S=\pm 1$. In contrast, in INS both intermultiplet and intramultiplet transitions can be observed ($\Delta S=0,\pm 1$, $\Delta M_S=0,\pm 1$). Thus, the combination of the two techniques allows assignment of all observed excitations.[18,19]

The determination of the model spin Hamiltonian parameters enabled us to estimate theoretically the effective energy barrier for the low spin molecule (1). Similarly to what we previously reported for the two high spin molecules (2) and (3), the results on (1) show how the presence of low-lying excited spin multiplets plays a crucial role in determining the relaxation of the magnetization.

In conventional systems, the effects of S mixing can be effectively modeled by the inclusion of fourth order zero-field splitting parameters in the giant spin Hamiltonian.[20] Here we will show that this Hamiltonian is completely inadequate for the description of the spin-state energy-level structure.

II. EXPERIMENTAL METHODS

Nondeuterated polycrystalline samples were synthesized according to published methods.[9,10] FDMR spectra were recorded on a previously described quasioptical spectrometer,[21] which employs backward wave oscillators as monochromatic coherent radiation sources and a Golay cell as detector. Sample (1) proved to deteriorate rapidly upon pressing and over time. Therefore, the FDMR measurements on (1) were performed on loose microcrystalline material (348 mg) held between two quartz plates. In this unconventional measurement, the detector signal was recorded as function of frequency at different temperatures. Extreme care had to be taken to prevent the slightest positional changes in sample and equipment, which changes the standing wave pattern in the beam, precluding normalization. The normalized transmission was calculated by dividing the signal intensity at a given temperature by that at the highest temperature (70 K). Samples (2) and (3) deteriorate to a lesser extent and FDMR spectra were recorded on pressed powder pellets made by pressing ca. 250 mg of the unground sample with approximately 50 mg n-eicosane (to improve pellet quality) into a pellet. All spectra were simulated using previously described software.[22]

INS experiments were performed using the multidisk-chopper time-of-fight spectrometers V3/NEAT at the Helmholtz-Zentrum Berlin für Materialien und Energie (HZB, Berlin, Germany) and IN5 and IN6 at the Institute Laue Langevin (Grenoble, France). The samples were inserted into hollow cylindric-shaped Aluminum containers and mounted inside a standard orange cryostat to achieve a base temperature of 2 K. A vanadium standard was used for the detector normalization and empty can measurements were used for the background subtraction.

III. THEORETICAL MODELING AND EXPERIMENTAL RESULTS

The experimental data have been modeled using both the giant spin Hamiltonian (GSH), which considers the ZFS of the ground-state multiplet only, and the microscopic spin Hamiltonian, which treats isotropic exchange and single-ion ZFS at the same level. Including only ZFS terms, the giant spin Hamiltonian for a spin state S reads

$$H_S = D_S\hat{S}_z^2 + E_S(\hat{S}_x^2 - \hat{S}_y^2) + B_4^0\hat{O}_4^0, \tag{1}$$

where D_S and E_S are second-order axial and transverse anisotropy, respectively, and B_4^0 is the fourth-order axial anisotropy, with $\hat{O}_4^0$ the corresponding Stevens operator. The microscopic spin Hamiltonian includes an isotropic exchange term for each pairwise interaction and single ion ZFS terms for each ion

$$H = \sum_{i<j} J_{ij}\mathbf{s}(i)\cdot\mathbf{s}(j) + \sum_i d_i s_z^2(i) + \sum_i \{35c_i s_z^4(i) + c_i[25 - 30s(s+1)]s_z^2(i)\}, \tag{2}$$

where $\mathbf{s}(i)$ are spin operators of the ith Mn ion. The first term is the isotropic exchange interaction while the second and third terms are the second- and fourth-order axial single-ion zero-field splitting, respectively (the z axis is assumed perpendicular to the plane of the triangle). The spin Hamiltonians have been numerically diagonalized by exploiting the conservation of the z component of the molecular total spin and the exchange and anisotropy parameters have been varied to obtain a best fit of the experimental data.

A. Mn_6 (1) ($S=4$) $U_{eff}\approx 28$ K

Sample (1) was the first reported member of the Mn_6 family.[16] The building block of the molecule is the $[Mn_3{}^{3+}O]$ triangular unit where Mn_2 pairs, bridged by the NO oxime, form a -Mn-O-N-Mn- moiety (Fig. 2).

The Mn-O-N-Mn torsion angles within each triangle are 10.7°, 16.48°, and 22.8°, giving rise to a dominant antiferromagnetic exchange coupling.[13] The two triangular units are coupled ferromagnetically, resulting in a total spin ground state of $S=4$. Four out of the six metal ions (Mn1, Mn2, Mn1′, and Mn2′) are six-coordinate and in distorted octahedral geometry (MnO_5N), with the Jahn-Teller axis almost perpendicular to the plane of the triangle, while the two remaining ions (Mn3 and Mn3′) are five-coordinate and in square pyramidal geometry (see Fig. 2). The effective energy barrier was determined from ac susceptibility measurements to be $U_{eff}=28$ K, with $\tau_0=3.6\times10^{-8}$ s (Ref. 16). From the effective energy barrier an estimate of $D\approx-0.15$ meV was derived.

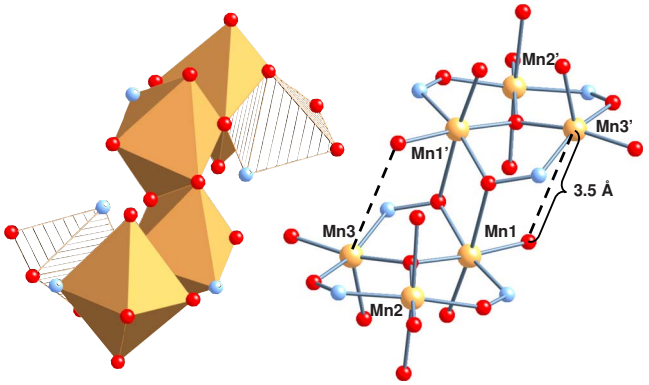

FIG. 2. (Color online) Structure of the Mn_6 (1) molecular core. The Mn^{3+} ions are located at the vertices of two oxocentered triangles. Ions Mn1, Mn2, Mn1′, and Mn2′ are in octahedral geometry and ions Mn3 and Mn3′ in square pyramidal geometry, as highlighted in filled and striped orange (left figure). Color scheme: Mn, large orange circles; O, dark red circles; and N, small light blue circles. H and C ions are omitted for clarity.

We performed INS and FDMR measurements to characterize the ground multiplet and to identify the position of the lowest-lying excited states from which we determine the effective exchange interaction and the zero-field splitting parameters. Figure 3 shows the FDMR spectra recorded on 350 mg unpressed powder of (1). The most pronounced feature is the resonance line at 1.803(7) meV while much weaker features can be observed at 1.328(1) and 1.07(1) meV. The intensity of the higher-frequency line is strongest at lowest temperature, proving that the corresponding transition originates from the ground-spin multiplet. The lower-frequency lines have maximum intensity at around 30 K. No further features were observed between 0.5 and 3 meV. The intense resonance line shows two shoulders to lower energies, which are much stronger in pressed powder samples and also increase with the age of the sample. This behavior is mirrored by the development of a pronounced asymmetric line shape in INS studies on older samples. We attribute these shoulders to microcrystalline particles that have suffered loss of lattice solvent, which leads to small conformational changes and this alters the ZFS and exchange parameters. We discard the possibility of isomers with different orientations of the Jahn-Teller distortion axes, as observed for Mn_{12},[23] because we see no signature of different isomers in the ac susceptibility. We also discount the possibility of closely spaced transitions, as observed in the Fe_{13} cluster,[24] because the intratriangle exchange interactions are not equal.

The higher-frequency resonance line is attributed to the transition from the $|S=4, M_S=\pm4\rangle$ to $|S=4, M_S\pm3\rangle$ states. INS measurements have found to be necessary to unambiguously identify the origin of the lower-frequency transitions (see below). Assuming that these transitions are transitions within the ground multiplet, a fit of the giant spin Hamiltonian ZFS parameters [Eq. (1)] to the observed resonance line energies yields $D_{S=4}=-2.12\pm0.03$ cm^{-1}

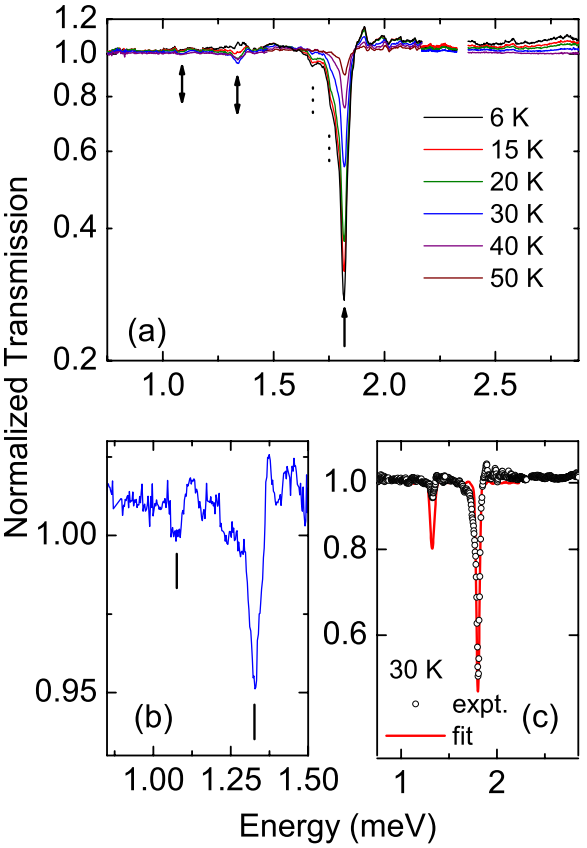

FIG. 3. (Color online) (a) FDMR spectra of unpressed polycrystalline powder of (1) recorded at various temperatures. The intensity of the higher-frequency resonance line decreases with temperature while that of the lower-frequency lines increases up to 30 K, beyond which it decreases again. Dotted lines indicate resonance lines due to impurities. (b) Expanded view of the low-frequency part of the 30 K spectrum. (c) Experimental and fitted spectrum at $T=30$ K using the GSH approximation. Note the logarithmic scale in (a) and (c).

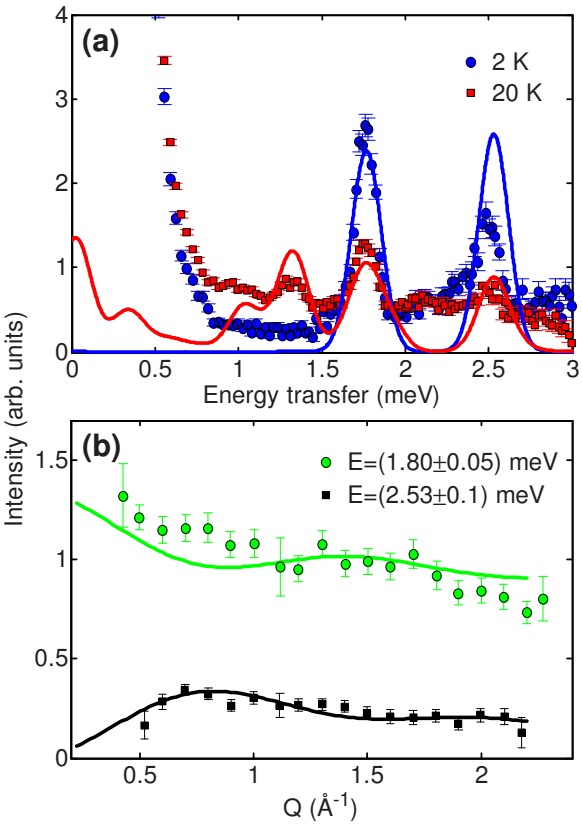

FIG. 4. (Color online) (a) INS spectra of (1) with an incident wavelength of $\lambda=4.6$ Å (NEAT) for $T=2$ K (blue circles) and $T=20$ K (red squares). The continuous lines represent the spectra calculated assuming a dimer model for the spin Hamiltonian [Eq. (3)]. (b) Q dependence of first intramultiplet (green circles) and intermultiplet (black squares) transitions measured on IN6 for $\lambda=4.1$ Å and $T=2$ K. Continuous lines represent the calculated Q dependence using the dimer spin Hamiltonian, Eq. (3), (assuming a dimer distance of $R=5.17$ Å, which corresponds to the distance between the center of the two triangles).

$(-0.263\pm0.004$ meV) and $B_4^0=+(1.5\pm0.5)\times10^{-4}$ cm^{-1} $(1.24\pm0.06\times10^{-5}$ meV). This ground state D_S value is much larger than reported spectroscopically determined D_S parameters for other manganese SMMs, e.g., $D_{S=10}=-0.457$ cm^{-1} for $Mn_{12}Ac$,[25] $D_{S=17/2}=-0.247$ cm^{-1} for Mn_9,[19] or $D_{S=6}=-1.16$ cm^{-1} for Mn_3Zn_2.[26] The main reason for this large D value is the fact that the projection coefficients for the single ion ZFS onto the cluster ZFS are larger for spin states with lower S (Ref. 27). The determined $D_{S=4}=-2.12$ cm^{-1} value for (1) is in excellent agreement with that found from density-functional-theory (DFT) calculations ($D=-2.15$ cm^{-1}).[28] The expected energy barrier toward relaxation of the magnetization calculated from the found spin Hamiltonian parameters is $U_{\text{theor}}=|D|S^2=48.8$ K, which is much larger than the experimentally found $U_{\text{eff}}\approx28$ K, indicating that more complex relaxation dynamics characterize this system, in analogy to what has been found for the Mn_6 $S=12$ compounds.[7] The linewidth of the 1.33 meV line is slightly larger than that of the 1.80 meV line (48 μeV versus 41 μeV), which can indicate the presence of more than one excitation. The simulated spectrum agrees very well for the higher-frequency resonance line (note that the intensity is not rescaled) while the lower-frequency line is much weaker in the experiment than from the fit. This can be tentatively attributed to the presence of low-lying excited states as observed previously for $Mn_{12}Ac$.[29] To determine the energy of excited spin states and identify the origin of the low-frequency resonances we resorted to INS, the technique of choice to directly access intermultiplet excitations.

The INS experiments were performed on ≈4 g of nondeuterated polycrystalline powder of (1), which was synthesized as described in Ref. 16. For our measurements we used incident neutron wavelengths ranging from 3.0 to 5.92 Å with energy resolution between 50 and 360 μeV.

Figure 4(a) shows the INS spectra for an incident wavelength of 4.6 Å collected on NEAT [210 μeV full width at half maximum (FWHM) resolution at the elastic peak]. At $T=2$ K, only the ground state is populated and therefore all excitations arise from the ground-state doublet $|S=4, M_S=\pm4\rangle$. We observed a strong transition at 1.77(2) meV, which we assign to the intramultiplet transition to the $|S=4, M_S=\pm3\rangle$ level, in agreement with FDMR results (see above). One further excitation was observed at higher energy at 2.53(1) meV.

At $T=20$ K, we detected additional excitations at 1.05(1) and 1.31(1) meV, which must be due to transitions from excited states. All peaks in the INS spectra show a very unusual asymmetric line shape, which we assign to lattice solvent loss (see above).

From the comparison of INS data with the FDMR results, we can deduce that the excitation at 2.53 meV has a pure intermultiplet origin, being absent in the FDMR spectra (see Fig. 3). This is also confirmed by the Q dependence of the scattering intensity of the observed excitations. Figure 4(b) shows this dependence for the $|S=4, M_S=\pm 4\rangle \rightarrow |S=4, M_S=\pm 3\rangle$ and $|S=4, M_S=\pm 4\rangle \rightarrow |S=3, M_S=\pm 3\rangle$ transitions. A characteristic oscillatory behavior has been observed for the Q dependence of the intermultiplet INS transition (black squares), which presents a maximum of intensity at a finite Q value (that is related to the geometry of the molecule), and decreasing intensity as Q goes toward zero. This Q dependence is typical for magnetic clusters and reflects the multispin nature of the spin states.[30,31] By contrast, the intramultiplet excitation (circles) has maximum intensity at $Q=0$, as expected for a transition with $\Delta S=0$, and the intensity decreases with increasing Q, following the magnetic form factor.

The INS data directly reveal the presence of low-lying excited multiplets. Indeed, the difference in energy between the lowest and the highest energy levels of the anisotropy split $S=4$ ground state is given, as a first approximation, by $|D|S^2=4.2$ meV. The presence of an intermultiplet excitation at only 2.53 meV energy transfer, therefore below 4.2 meV, indicates that the first excited S multiplet lies within the energy interval of the anisotropy split $S=4$ state. This suggests that the observed low-energy excitations are possibly not pure intramultiplet transitions but are expected to originate from the $S=4$ ground state and from the first excited S multiplet. Therefore the exact assignment of those excitations requires a more accurate analysis beyond the GSH approximation. Indeed, one fundamental requirement for the validity of the GSH approximation, i.e., an isolated ground state well separated from the excited states, is not fulfilled and S is not a good quantum number to describe the ground state of the molecule. To model the data it is thus necessary to use the full microscopic spin Hamiltonian of Eq. (2). This situation is also encountered in other studied molecules, such as, for example, in Mn_{12},[32–36] in the Mn-$[3\times 3]$ grid,[37,38] in Ni_4,[39] and in V_{15},[33,35,40] where the detailed modeling of the experimental results has required the use of a multispin approach.

Given the low symmetry of the triangular units in (1), the number of free parameters in Eq. (2) would be too large to obtain unambiguous results, considering the low number of experimentally observed excitations. Hence, we have chosen to describe the low-energy physics of (1) by a simplified dimer model, an approximation which has already previously been adopted for (3) (see Ref. 41). The dimer model was found to reproduce correctly the experimental results for molecule (3) and the calculated low-energy spectrum was found to be consistent with the one obtained using the microscopic spin Hamiltonian. In molecule (1) the small Mn-O-N-Mn torsion angles suggest a large dominant antiferromagnetic interaction within each triangle, as predicted by DFT calculations.[17] The two triangular units can be therefore

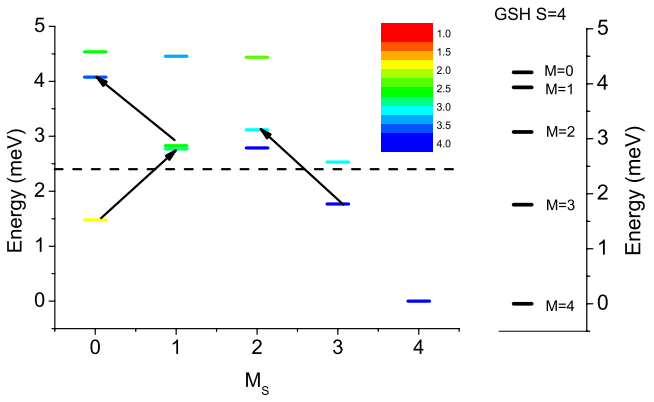

FIG. 5. (Color online) Calculated energy-level diagram for molecule (1). The level scheme on the left side is calculated using the dimer model spin Hamiltonian in Eq. (3). The color maps S_{eff}, where $\langle S^2\rangle := S_{\text{eff}}(S_{\text{eff}}+1)$. The black dashed line corresponds to the observed value of $U_{\text{eff}}=28$ K. The black arrows indicate transitions which contribute to the observed peak in the INS and FDMR spectra at $E\approx 1.33$ meV (see text for details). The level diagram on the right has been calculated using the GSH approximation [Eq. (1)].

described as two ferromagnetically coupled $S=2$ spins, which also experience an effective uniaxial crystal-field (CF) potential

$$H_{dimer} = J(\mathbf{S}_A \cdot \mathbf{S}_B) + d(S_{A,z}^2 + S_{B,z}^2). \tag{3}$$

The spin Hamiltonian has been diagonalized numerically and the J and d parameters have been varied to obtain a best fit of the experimental data. The position of the peak at 1.77 meV does not depend on the exchange interaction, therefore its position sets the value of the axial anisotropy d parameter. Given the d parameter, a fit of the position of the peak at 2.53 meV sets the isotropic exchange parameter J.

The best fit of the experimental data is obtained with $J=-0.19$ meV and $d=-0.59$ meV. The calculated energy-level scheme is reported in Fig. 5 (left), where the comparison with the energy-level diagram in the GSH approximation is also reported (right). The value of S_{eff} [where $\langle S^2\rangle := S_{\text{eff}}(S_{\text{eff}}+1)$] is labeled in color and shows that the first $S=3$ excited state is completely nested within the $S=4$ ground state. From Fig. 5 it is also clear that the GSH model does not account for a number of spin states different from the ground state $S=4$ multiplet at low energy. Furthermore, the assignment of the observed excitations can be misleading if considering the GSH approximation only. For example, using the GSH model, the observed peak at 1.33 meV can only be attributed to a pure intramultiplet excitation from $|4,\pm 3\rangle$ to $|4,\pm 2\rangle$, while using Eq. (3), it is found to be a superposition of several intermultiplet and intramultiplet transitions (indicated by arrows in Fig. 5). The GSH approximation fails to describe the low energy-level diagram of the molecule and consequently fails to describe the relaxation of the magnetization. Indeed, the presence of excited states nested within the ground state multiplet has a significant effect on the relaxation dynamics, as discussed in Sec. IV.

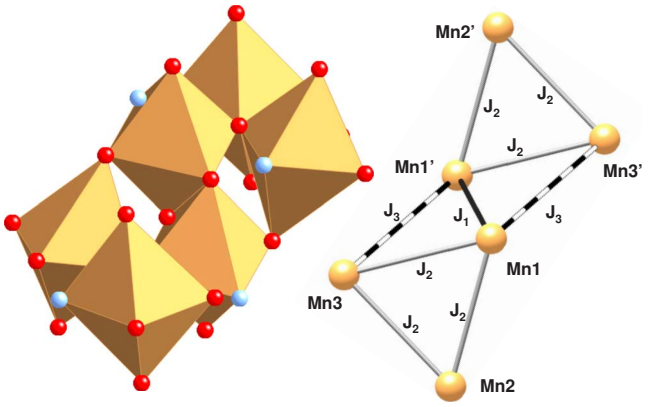

FIG. 6. (Color online) Structure of the Mn_6 (2) molecular core. The Mn^{3+} ions are located at the vertices of two oxocentered triangles. All Mn ions are in octahedral geometry and the octahedra are highlighted in orange (left figure). Color scheme: Mn, large orange circles; O, dark red circles; and N, small light blue circles. H and C ions are omitted for clarity. On the right, a schematic representation is given, together with the exchange coupling scheme adopted for the spin Hamiltonian calculations.

B. Mn_6 (2) $U_{eff}\approx 53$ K vs Mn_6 (3) $U_{eff}\approx 86.4$ K

Introducing sterically more demanding oximate ligands results in a twisting of the Mn-N-O-Mn torsion angle,[9] which causes switching of the intratriangle exchange interactions from antiferromagnetic to ferromagnetic, resulting in a large increase in the spin of the ground state from $S=4$ to $S=12$. Here, we study two [(2) and (3), respectively] of the many published derivatives of these $S=12$ Mn_6 clusters. Compound (2) has undergone two structural changes compared to (1). First of all, the distance between the phenolato oxygen and the two square pyramidal Mn^{3+} ions has decreased from ≈ 3.5 to ≈ 2.5 Å, thus all Mn^{3+} ions are now in six-coordinated distorted octahedral geometry (see Fig. 6). Second, the torsion angles of the Mn-N-O-Mn moieties has increased strongly with respect to those in (1), being 38.20°, 39.9°, and 31.26°, compared to 10.7°, 16.48°, and 22.8° for (1). In (3), the introduction of two methyl groups on the carboxylate ligand has increased the nonplanarity of the Mn-N-O-Mn moieties further, giving torsion angles of 39.08°, 43.07°, and 34.88°.[10] The result is that the weakest ferromagnetic coupling is significantly stronger for (3) compared to (2). Using a single J model (e.g., assuming that the intratriangle and intertriangle exchange couplings are equal), Milios *et al.*[12,14] fitted the dc susceptibility data for molecules (2) and (3) and obtained: $J(2)=-0.230$ meV and $J(3)=-0.404$ meV, respectively, (in our notation for the spin Hamiltonian).

In spite of the fact that both (2) and (3) have $S=12$ ground states and similar geometrical structures, radically different effective energy barriers toward the relaxation of the magnetization were observed, being $U_{eff}\approx 53$ K for (2) and $U_{eff}\approx 86.4$ K for (3). Here, we aim to understand this difference by an in-depth study of the energy-level structure by means of FDMR and INS.

Figure 7 shows FDMR spectra recorded on a pressed powder pellet of (2) at different temperatures. The baseline

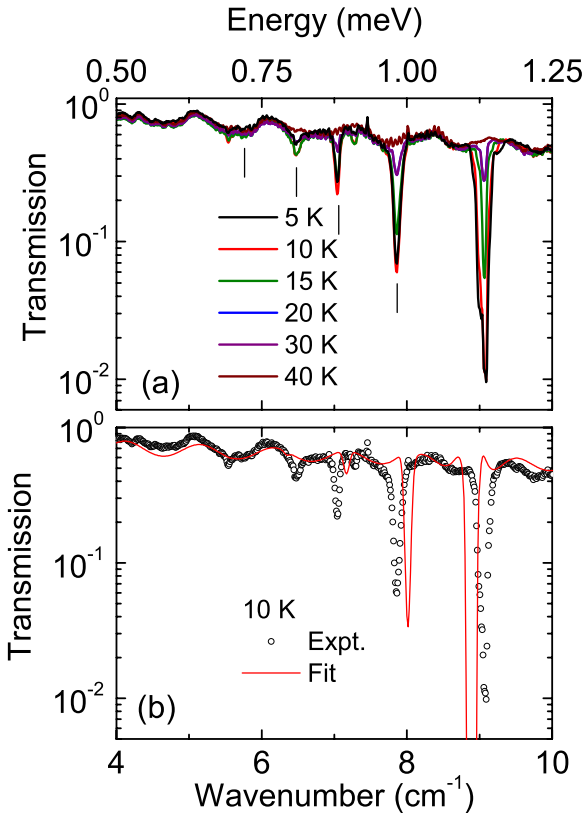

FIG. 7. (Color online) (a) FDMR spectra recorded on a pressed powder pellet of 2 at different temperatures. At the lowest temperature, the highest-frequency line has highest intensity. The other transitions are indicated by vertical lines. (b) 10 K FDMR spectrum (symbols) and best fit using the GSH [Eq. (1)] with $D=-0.368$ cm^{-1} and $B_4^0=-4.0\times 10^{-6}$ cm^{-1}.

shows a pronounced oscillation, which is due to Fabry-Pérot-type interference within the plane-parallel pellet.[22] The oscillation period and downward slope to higher frequencies are determined by the thickness of the pellet and the complex dielectric permittivity, which were determined to be $\epsilon'=3.01$ and $\epsilon''=0.049$, values typical for molecular magnet samples. In addition, five resonance lines are observed which we attribute to resonance transitions within the $S=12$ multiplet. Thus, the highest-frequency line is assigned to the $|12,\pm 12\rangle \rightarrow |12,\pm 11\rangle$ transition, and so on. The lines are much narrower (11 μeV FWHM) than those observed for other SMMs, e.g., 23 μeV FWHM for Mn_{12}Ac. The fit procedure showed that the lines are inhomogeneously broadened and best described by Gaussian line shapes. The small linewidth indicates that distributions in ZFS parameters (D strain) are small in these samples. A fit of the GSH parameters [Eq. (1)] to the observed resonance frequencies, yields $D_{S=12}=-0.368$ cm^{-1} (0.0456 meV) and $B_4^0=-4.0\times 10^{-6}$ cm^{-1} (4.96×10^{-7} meV) best parameter values. The theoretical energy barrier calculated from these ZFS parameters is $U_{theor}=76$ K, which is much larger than the experimentally found $U_{eff}\approx 53$ K, indicating that the molecule can shortcut the barrier in some way. The ZFS values are in themselves not remarkable and close to those reported for other manganese clusters with similar ground state spins,

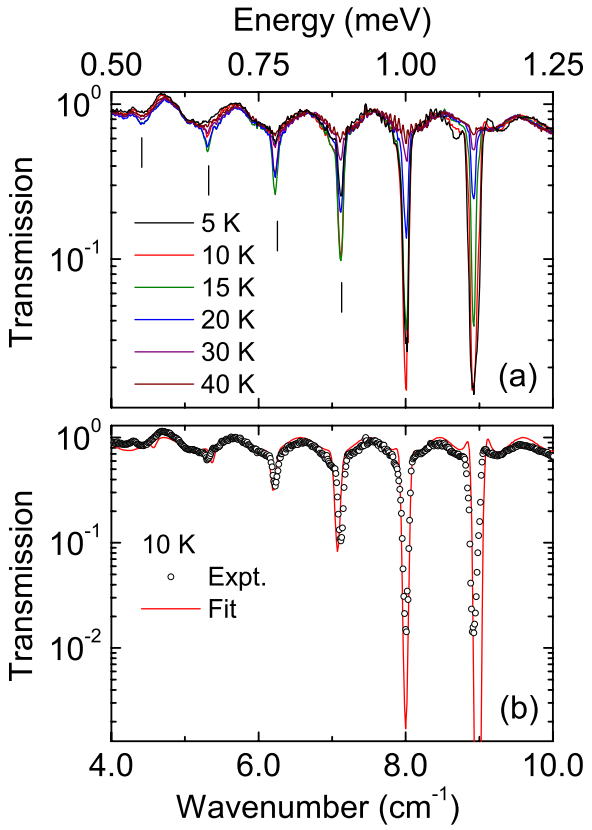

FIG. 8. (Color online) (a) FDMR spectra of unpressed polycrystalline powder of (3) recorded at various temperatures. (b) Experimental and fitted spectrum at $T=10$ K.

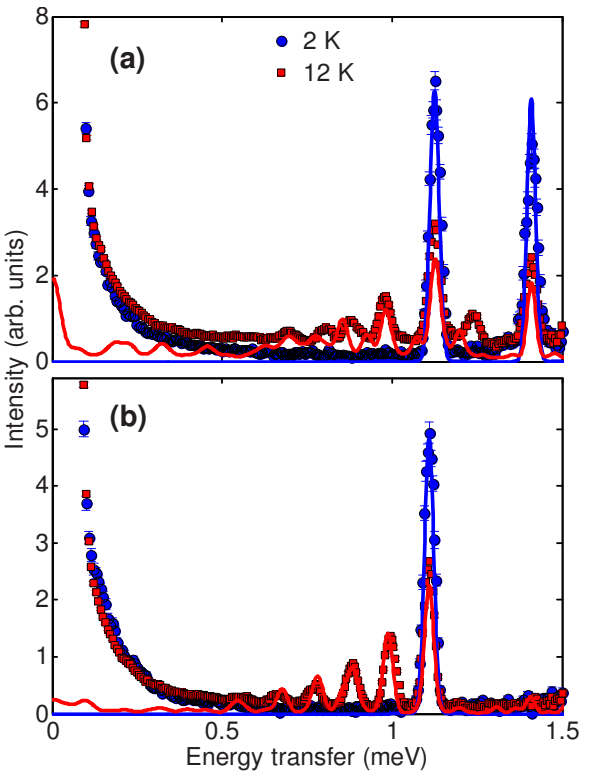

FIG. 9. (Color online) INS spectra collected on IN5 with incident wavelength of 6.7 Å at $T=2$ K (blue circles) and $T=12$ K (red squares). (a) for sample (2) and (b) for sample (3). The spectra calculated with the parameters listed in Table II are shown as continuous lines.

e.g., $D_{S=10}=-0.457$ cm^{-1} for $Mn_{12}Ac$ (Ref. 25) and $D_{S=17/2}=-0.247$ cm^{-1} for Mn_9.[19] Interestingly, the fourth-order axial ZFS is an order of magnitude smaller than for $Mn_{12}Ac$. This type of ZFS is currently accepted to parametrize effects of mixing between spin multiplets (S mixing),[42] which would mean that S mixing is only limited, contrary to expectation. However, the fit does not simulate the resonance line positions and intensities satisfactorily, which is in contrast to the situation for other molecular nanomagnets that feature strong S mixing, e.g., Ni_4.[18,43] Therefore, the investigated Mn_6 SMM represents an example where the giant spin model cannot satisfactorily describe FDMR spectra and it will be shown below that this is due to a complete breakdown of the giant spin model. It will also be shown that the resonance line at 0.80 meV is due to a transition within the $S=11$ excited multiplet. However, removal of this resonance line does not result in a better fit. The calculated line intensities are much larger than those experimentally found, especially for the highest-frequency lines. This we attribute to a combination of parasitic radiation in the cryostat, and the presence of many more states than taken into account by the giant spin model, which decreases the relative population for any given state.

Similar FDMR results were obtained for (3) (Fig. 8) and six sharp resonance lines were observed. A fit of the GSH parameters to the observed resonance line positions yields the following values: $D=-0.362\pm0.001$ cm^{-1} (-0.0449 meV) and $B_4^0=-6.0\pm0.4\times10^{-6}$ cm^{-1} (-7.4×10^{-7} meV). The simulated spectrum matches the experiment much more closely for (3), especially for the high-frequency lines. Interestingly, the theoretical energy barrier ($U_{\text{theor}}=75$ K) is virtually the same as for (2) but *smaller* than the experimentally found energy barrier ($U_{\text{eff}}=86$ K). This unprecedented finding means that the magnetization relaxation must involve states that do not belong to the ground-spin multiplet.[7] Again, we turn to INS to determine the positions of the excited-spin multiplets, which will allow full characterization of the system.

Figures 9(a) and 9(b) show the high-resolution INS experimental data for compounds (2) and (3), respectively, collected on IN5 with an incident wavelength of 6.7 Å (53 μeV FWHM resolution at the elastic peak). At the lowest temperature $T=2$ K only the ground state is populated and, due to the INS selection rules, only transitions with $\Delta S=0,\pm1$ and $\Delta M=0,\pm1$ can be detected. The lowest-energy excitation can be thus easily attributed to the intramultiplet transition from the $|S=12,\ M_S=\pm12\rangle$ ground state to the $|S=12,\ M_S=\pm11\rangle$ first excited level. The position of this intramultiplet excitation is found to be at about the same energy in both compounds, i.e., ~1.1 meV, indicating only small differences in the anisotropy of the two systems. In contrast the first intermultiplet $S=12\rightarrow S=11$ excitation at about 1.41 meV in compound (2) is not visible in the spectra at 6.7 Å of compound (3). This can be understood looking at the data at higher-energy transfer, collected with an incident wavelength of 3.4 Å [see Figs. 10(a) and 10(b)]. Indeed the

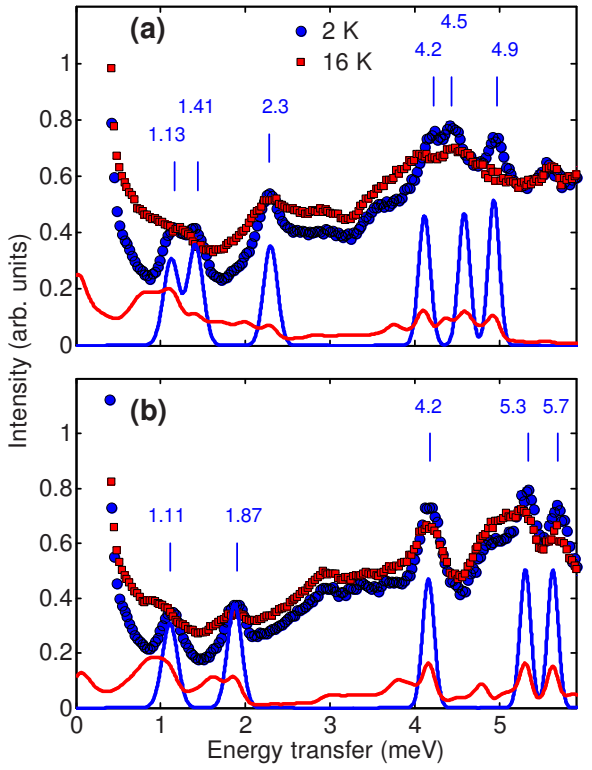

FIG. 10. (Color online) INS spectra collected on IN5 with incident wavelength of 3.4 Å at $T=2$ K (blue circles) and 16 K (red squares). (a) for sample (2) and (b) for sample (3). The observed transitions are labeled with the corresponding transition energies in meV.

first intermultiplet excitation is considerably raised in energy in compound (3) with respect to compound (2), from 1.41 to 1.87 meV. This gives a direct evidence of an increase in the isotropic exchange parameters while the anisotropic parameters are approximately the same for both molecules. The INS spectra collected at a base temperature of 2 K, enabled us to directly access the whole set of intramultiplet and intermultiplet transitions allowed by the INS selection rules in both compounds. By raising the temperature to 16 K the intensity of the magnetic peaks decreases, thus confirming their magnetic origin. A total of five intermultiplet excitations for compound (2) toward different $S=11$ excited states can be detected. For compound (3) four intermultiplet excitations have been observed. All the magnetic excitations are marked in Fig. 10 with the corresponding transition energies.

To complete our investigations of the transitions within the $S=12$ ground-state multiplet, we additionally performed high-resolution measurements of molecule (3) using IN5 with incident wavelengths of 10.5 Å (FWHM=13 μeV at the elastic line) (see Fig. 11). These measurements allowed us to observe transitions originating from the top of the anisotropy barrier.

A further confirmation of the good assignment of the observed excitations is provided by the study of their Q dependence. As revealed by Fig. 12, the intramultiplet transition ($\Delta S=0$) shows a distinctive Q dependence, with a pronounced intensity at low Q, that dies out quite rapidly following the Mn^{3+} form factor. In contrast, intermultiplet excitations present flatter behavior with considerably less intensity at low Q. The assignment of the observed excitations to intramultiplet or intermultiplet transitions has been confirmed by comparison with FDMR measurements performed on both compounds (see Figs. 7 and 8). The position

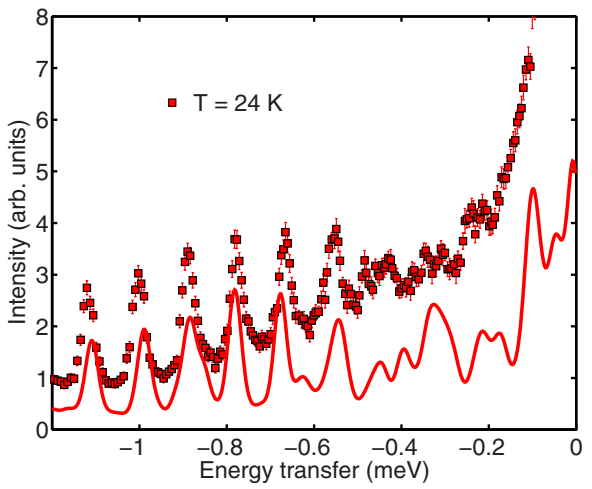

FIG. 11. (Color online) High-resolution INS spectra of molecule (3) collected on IN5 with incident wavelength 10.5 Å at 24 K. The energy gain spectra is displayed. Continuous lines are the calculations using the spin Hamiltonian of Eq. (2).

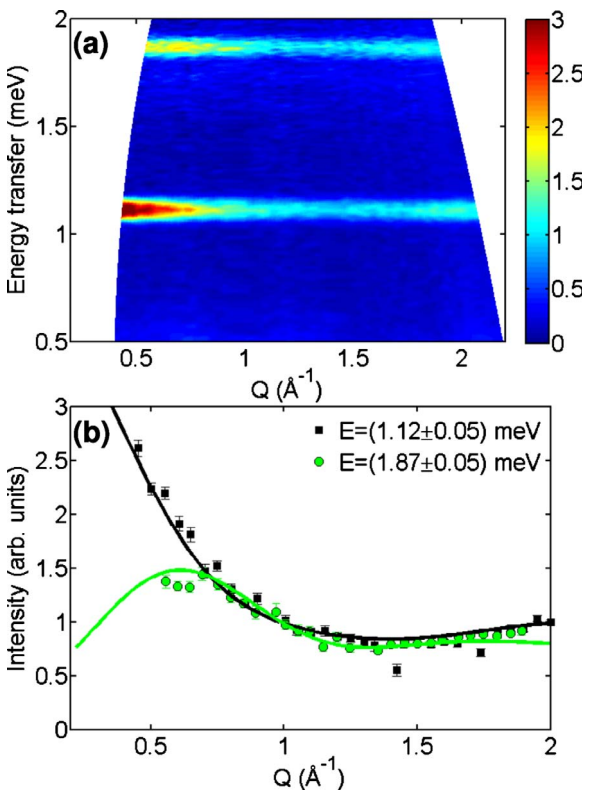

FIG. 12. (Color online) (a) Energy-wave vector color map of sample (3) collected on IN5 with incident wavelength of 5.0 Å. (b) Q dependence of two transitions from the ground state. The black squares correspond to the $|S=12,\ M_s=\pm 12\rangle \rightarrow |S=12,\ M_s=\pm 11\rangle$ intramultiplet transition and the green circles display the $|S=12,\ M_s=\pm 12\rangle \rightarrow |S=11,\ M_s=\pm 11\rangle$.

TABLE I. INS and FDMR peak positions of the observed excitations for (2) and (3) (in meV).

(2)	INS	FDMR	(3)	INS	FDMR
	4.9(2)	N.O.[a]		5.7(2)	N.O.
	4.5(1)	N.O.		5.3(2)	N.O.
	4.2(2)	N.O.		4.2(2)	N.O.
	2.3(2)	N.O.		1.87(3)	N.O.
	1.41(2)	N.O.		1.11(1)	1.107(7)
	1.24(7)	N.O.		0.99(1)	0.993(6)
	1.13(2)	1.127(5)		0.88(2)	0.883(6)
	0.98(2)	0.975(5)		0.77(1)	0.772(7)
	0.88(3)	0.873(6)		0.66(1)	0.657(7)
	0.80(2)	0.803(7)		0.55(2)	0.551(10)
	0.70(2)	0.687(5)		0.48(1)	N.O.
	0.57(4)	N.O.		0.45(1)	N.O.
				0.34(1)	N.O.
				0.31(1)	N.O.
				0.25(1)	N.O.
				0.21(3)	N.O.

[a]Not observed.

of the intramultiplet INS transitions are consistent with the FDMR measurements performed on the same sample (see Table I). Due to the different selection rules of INS and FDMR, we can conclude that all the peaks observed at $T=2$ K above 1.2 meV energy transfer correspond to intermultiplet transitions since they are absent in the FDMR spectra.

The straightforward assignment of the base temperature observed excitations allows us to draw some considerations on the experimentally deduced energy-level diagram. For both compounds, a rough estimate of the splitting of the spin ground multiplet gives $|D|S^2 \simeq 6.5$ meV. This value is comparable to the energy interval explored by the high-energy transfer INS data (Fig. 10), where most of the intermultiplet $S=12 \rightarrow S=11$ excitations have been observed. This experimental observation leads to the conclusion that also in (2) and (3) several excited states lie within the anisotropy split ground state with the consequent breakdown of the GSH approximation. Due to the inadequacy of the GSH for (2) and (3), the microscopic spin Hamiltonian [Eq. (2)] was used to model the data and extract the exchange constants and anisotropies. The minimal set of free parameters is given by three different exchange constants $J_{11'} \equiv J_1$, $J_{12}=J_{23}=J_{13}=J_{1'2'}=J_{2'3'}=J_{1'3'} \equiv J_2$, and $J_{13'}=J_{1'3} \equiv J_3$ (Fig. 6) and two sets of CF parameters $d_1=d_{1'}$, $c_1=c_{1'}$, and $d_2=d_{2'}$, $c_2=c_{2'}$. Indeed, the ligand cages of sites 1 and 3 are rather similar and we assumed the corresponding CF parameters to be equal. Since experimental information is insufficient to fix independently the two small c parameters, we have chosen to constrain the ratio c_1/c_2 to the ratio d_1/d_2.

The isotropic exchange and crystal-field parameters deduced by the simultaneous best fit of the experimental data are reported in Table II. Figure 13 shows the calculated energy-level diagram using the best fit procedure for Eq. (2) (left) and the GSH model (right) for (2) and (3).

IV. DISCUSSION

The experimental data collected on the three variants of Mn_6 clusters provide direct evidence that a general feature for this class of compounds is the nesting of excited multiplets within the ground-state multiplet. This is an unavoidable effect when the isotropic exchange parameters have the same order of magnitude as the single ion anisotropy parameters, as it happens to be for Mn_6. The nesting of spin states can be clarified by observing the energy-level diagrams for the three molecules presented in Figs. 5 and 13. The diagram on the left shows the energy levels calculated by a diagonalization of the full spin Hamiltonian while the energy-level scheme on the right-hand side has been calculated considering the GSH approximation. It is clear that the GSH does not account for any of the spin states with S different from S_{GS} that lie within the split GS energy-level diagram. The above states represent a shortcut for the relaxation of the magnetization and can promote resonant intermultiplet tunneling processes that manifest as additional steps in the magnetization curve absent in the GS model.[8,41,44–46] The overall result is a lowering of the effective anisotropy barrier with respect to an ideal molecule where the spin ground state is well separated from the excited ones, as was first demonstrated in Ref. 7.

TABLE II. Isotropic exchange and CF parameters for Eq. (2) (in meV) deduced by fitting INS and FDMR data for the two Mn_6 $S=12$ compounds.

	U_{eff} (K)	J_1	J_2	J_3	d_1	d_2	c_1
(2)	53	−0.61	−0.31	0.07	−0.23	−0.97	−0.0008
(3)	86.4	−0.84	−0.59	0.01	−0.20	−0.76	−0.001

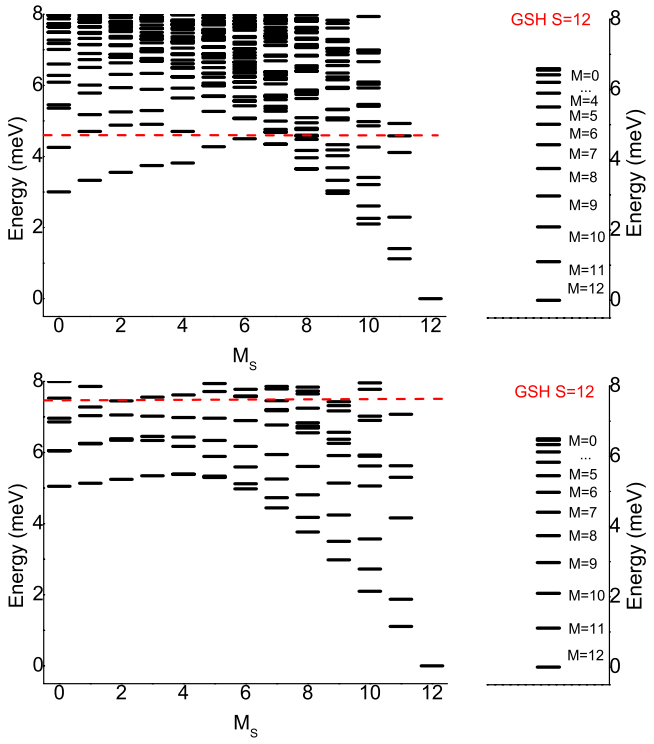

FIG. 13. (Color online) Calculated energy-level diagram for molecule (2) (top) and molecule (3) (bottom). The level scheme on the left side is calculated using the microscopic spin Hamiltonian in Eq. (2) while the level diagram on the right has been calculated in the GSH approximation [Eq. (1)]. The dashed lines correspond to the observed value of U_{eff}.

We have calculated the relaxation dynamics of molecule (1) following the same procedure adopted in Ref. 7 for molecules (2) and (3). We applied a master equations formalism in which the magnetoelastic coupling is modeled as in Ref. 47 with the quadrupole moments associated to each triangular unit isotropically coupled to Debye acoustic phonons. The transition rates W_{st} between pairs of eigenlevels of the dimer spin Hamiltonian, Eq. (3), is given by

$$W_{st} = \gamma^2 \Delta_{st}^3 n(\Delta_{st}) \sum_{A,B,q_1,q_2} \langle s|O_{q_1,q_2}(\mathbf{S}_A)|t\rangle \overline{\langle s|O_{q_1,q_2}(\mathbf{S}_B)|t\rangle}, \tag{4}$$

where $O_{q_1,q_2}(\mathbf{S}_{A,B})$ are the components of the Cartesian quadrupole tensor operator, $n(\Delta_{st}) = (e^{\hbar\Delta_{st}/k_BT} - 1)^{-1}$ and $\Delta_{st} = (E_s - E_t)/\hbar$. We found out that the resulting relaxation spectrum at low T is characterized by a single dominating relaxation time whose T dependence displays a nearly Arrhenius behavior $\tau = \tau_0 \exp(U/k_BT)$, as previously observed for molecules (2) and (3).[7] The relaxation dynamics of M is indeed characterized by two separated time scales: fast processes that determine the equilibrium within each well of the double-well potential and a slow interwell process that at low temperature determines the unbalancing of the populations of the two wells and thus sets the time scale for the reversal of the magnetization.[5,6] As can be observed from the energy-level diagram of Fig. 5 there are several levels that can be involved in the interwell relaxation process, giving rise to an overall effective barrier U_{eff} different from the simple energy difference between the $M=0$ and $M=\pm 4$ states. The corresponding calculated energy barrier $U_{\text{calc}}=32$ K reproduces quite well the experimental value, $U_{\text{eff}}=28$ K. The lowering of the barrier is therefore attributed to the presence of these extra paths. Indeed, the calculations for artificially isolated $S=4$ yield $U=47$ K.

It is worth commenting also on the D value for the ground state of each molecule. While no large difference between the local d of the low (1) and high [(2) and (3)] spin molecules is expected, the overall D value, as determined using the GSH approximation, is much higher for the $S=4$ molecule ($D \approx -0.263$ meV) than for the high spin molecules ($D \approx -0.045$ meV). However, this observation should not be misinterpreted. The difference arises from the fact that D depends on the projection of the individual single-ion anisotropies of each magnetic ion onto the total spin quantum number S. In the case where the S mixing is negligible and the spin ground state is a good quantum number, the D parameter for a specific state S can be written as linear combination of the single-ions anisotropy tensors (Ref. 27)

$$\mathbf{D} = \sum_{i=1}^{N} a_i \mathbf{d}_i. \tag{5}$$

The projection coefficients a_i of the single ion anisotropy to spin states of different S values can differ significantly, giving rise to considerably different D values. The ligand field study of various members of the Mn_6 family (Ref. 48) provides experimental evidence of this. Recent theoretical studies proposed that the intrinsic relationship between S and D causes a scaling of U that goes approximately with S^0 (see Refs. 4 and 28), raising the question whether it is worth trying to increase the value of spin ground state to obtain a larger energy barrier. Indeed, higher spin ground states would correspond to lower D parameters, neutralizing the overall effect on the height of the anisotropy barrier. In recently performed electron paramagnetic resonance studies the authors proposed that the barrier goes roughly with S^1 instead.[49] In the specific case of Mn_6, because of the very large S mixing, the projection onto a well-defined spin state is no more justified and it is not possible to associate the barrier U to a defined S value. However, if we consider the effective anisotropy barrier for artificially isolated $S=4$ and $S=12$ states [i.e., $U=47$ K for (1) and $U=105$ K for (2)], we can confirm that the barrier does not go quadratically with S, as one could naively deduce from the equation $U = |D|S^2$. Indeed, $U_{S=12}/U_{S=4} = 2.2 \ll 12^2/4^2 = 9$. This confirms what has been pointed out in Ref. 4, i.e., even though the highest anisotropy barrier is obtained with the molecule with the highest spin ground state, the increase in the total spin is not as efficient as one would expect and alternative routes, such as increasing the single ion anisotropy, should be considered.

V. CONCLUSION

We have performed INS and FDMR measurements on three variants of Mn_6 molecular nanomagnets, which have

the same magnetic core and differ by slight changes in the organic ligands. INS measurements have unambiguously evidenced the presence of low-lying excited states in all the three molecules. The combination of the two techniques enabled us to determine the spin Hamiltonian parameters used for the analysis of the magnetic properties. The nesting of excited states within the ground-state multiplet strongly influences the relaxation behavior and plays a crucial role in lowering the effective energy barrier. The calculations of the relaxation dynamics give results that are consistent with the experimental values and show that the highest barrier is obtained for ideal molecules with an isolated ground state. This observation might be valid for a wider class of SMMs and suggests that the combination of a high uniaxial anisotropy together with strong intramolecular exchange interactions is necessary to hinder the relaxation of the magnetization and engineer molecules able to retain the magnetization for a long time.

ACKNOWLEDGMENTS

This work was partly supported by EU-RTN QUEMOLNA under Contract No. MRTN-CT-2003-504880, the German Science Foundation DFG, and EPSRC. This work utilized facilities supported in part by the National Science Foundation under Agreement No. DMR-0454672.

*oliver.pieper@helmholtz-berlin.de
†tatiana.guidi@stfc.ac.uk

[1] R. Sessoli, D. Gatteschi, A. Caneschi, and M. A. Novak, Nature (London) **365**, 141 (1993).
[2] N. E. Chakov, S.-C. Lee, A. G. Harter, P. L. Kuhns, A. P. Reyes, S. O. Hill, N. S. Dalal, W. Wernsdorfer, K. Abboud, and G. Christou, J. Am. Chem. Soc. **128**, 6975 (2006).
[3] J. Villain, F. Hartman-Boutron, R. Sessoli, and A. Rettori, Europhys. Lett. **27**, 159 (1994).
[4] O. Waldmann, Inorg. Chem. **46**, 10035 (2007).
[5] A. Würger, J. Phys.: Condens. Matter **10**, 10075 (1998).
[6] D. Zueco and J. L. Garcia-Palacios, Phys. Rev. B **73**, 104448 (2006).
[7] S. Carretta *et al.*, Phys. Rev. Lett. **100**, 157203 (2008).
[8] S. Carretta *et al.*, Polyhedron **28**, 1940 (2009).
[9] C. J. Milios, A. Vinslava, P. A. Wood, S. Parsons, W. Wernsdorfer, G. Christou, S. P. Perlepes, and E. K. Brechin, J. Am. Chem. Soc. **129**, 8 (2007).
[10] C. J. Milios, A. Vinslava, W. Wernsdorfer, S. Moggach, S. Parsons, S. P. Perlepes, G. Christou, and E. K. Brechin, J. Am. Chem. Soc. **129**, 2754 (2007).
[11] C. J. Milios, A. Vinslava, W. Wernsdorfer, A. Prescimone, P. A. Wood, S. Parsons, S. P. Perlepes, G. Christou, and E. K. Brechin, J. Am. Chem. Soc. **129**, 6547 (2007).
[12] R. Inglis *et al.*, Dalton Trans. **2009**, 3403.
[13] C. J. Milios, S. Piligkos, and E. K. Brechin, Dalton Trans. **2008**, 1809.
[14] C. J. Milios, R. Inglis, A. Vinslava, R. Bagai, W. Wernsdorfer, S. Parsons, S. P. Perlepes, G. Christou, and E. K. Brechin, J. Am. Chem. Soc. **129**, 12505 (2007).
[15] A. Prescimone *et al.*, Dalton Trans. **2009**, 4858.
[16] C. J. Milios, C. P. Raptopoulou, A. Terzis, F. Lloret, R. Vicente, S. P. Perlepes, and A. Escuer, Angew. Chem. Int. Ed. **43**, 210 (2004).
[17] E. Cremades, J. Cano, E. Ruiz, G. Rajaraman, C. J. Milios, and E. K. Brechin, Inorg. Chem. **48**, 8012 (2009).
[18] A. Sieber *et al.*, Inorg. Chem. **44**, 4315 (2005).
[19] S. Piligkos *et al.*, J. Am. Chem. Soc. **127**, 5572 (2005).
[20] E. Liviotti, S. Carretta, and G. Amoretti, J. Chem. Phys. **117**, 3361 (2002).
[21] J. van Slageren *et al.*, Phys. Chem. Chem. Phys. **5**, 3837 (2003).
[22] N. Kirchner, J. van Slageren, and M. Dressel, Inorg. Chim. Acta **360**, 3813 (2007).
[23] S. Aubin, Z. Sun, H. Eppley, E. Rumberger, I. Guzei, K. Folting, P. Gantzel, A. Rheingold, G. Christou, and D. Hendrickson, Inorg. Chem. **40**, 2127 (2001).
[24] J. van Slageren *et al.*, Phys. Rev. B **73**, 014422 (2006).
[25] I. Mirebeau, M. Hennion, H. Casalta, H. Andres, H. U. Güdel, A. V. Irodova, and A. Caneschi, Phys. Rev. Lett. **83**, 628 (1999).
[26] P. L. Feng, C. Koo, J. J. Henderson, M. Nakano, S. Hill, E. del Barco, and D. N. Hendrickson, Inorg. Chem. **47**, 8610 (2008).
[27] A. Benicni and D. Gatteschi, *Electron Paramagnetic Resonance of Exchange Coupled Clusters* (Springer, Berlin, 1990).
[28] E. Ruiz, J. Cirera, J. Cano, S. Alvarez, C. Loose, and J. Kortus, Chem. Commun. **2008**, 52.
[29] J. van Slageren, S. Vongtragool, B. Gorshunov, A. Mukhin, and M. Dressel, Phys. Rev. B **79**, 224406 (2009).
[30] A. Furrer and H. U. Güdel, Phys. Rev. Lett. **39**, 657 (1977).
[31] O. Waldmann, Phys. Rev. B **68**, 174406 (2003).
[32] M. I. Katsnelson, V. V. Dobrovitski, and B. N. Harmon, Phys. Rev. B **59**, 6919 (1999).
[33] G. Chaboussant, R. Basler, A. Sieber, S. T. Ochsenbein, A. Desmedt, R. E. Lechner, M. T. F. Telling, P. Kögerler, A. Müller, and H.-U. Güdel, Europhys. Lett. **59**, 291 (2002).
[34] H. A. De Raedt, A. H. Hams, V. V. Dobrovitski, M. Al-Saqer, M. I. Katsnelson, and B. N. Harmon, J. Magn. Magn. Mater. **246**, 392 (2002).
[35] H. De Raedt, S. Miyashita, K. Michielsen, and M. Machida, Phys. Rev. B **70**, 064401 (2004).
[36] O. Waldmann and H.-U. Güdel, Phys. Rev. B **72**, 094422 (2005).
[37] T. Guidi *et al.*, Phys. Rev. B **69**, 104432 (2004).
[38] O. Waldmann, S. Carretta, P. Santini, R. Koch, A. G. M. Jansen, G. Amoretti, R. Caciuffo, L. Zhao, and L. K. Thompson, Phys. Rev. Lett. **92**, 096403 (2004).
[39] A. Wilson, J. Lawrence, E. C. Yang, M. Nakano, D. N. Hendrickson, and S. Hill, Phys. Rev. B **74**, 140403(R) (2006).
[40] J. Kortus, C. S. Hellberg, and M. R. Pederson, Phys. Rev. Lett. **86**, 3400 (2001).
[41] S. Bahr, C. J. Milios, L. F. Jones, E. K. Brechin, V. Mosser, and W. Wernsdorfer, Phys. Rev. B **78**, 132401 (2008).
[42] S. Carretta, E. Liviotti, N. Magnani, P. Santini, and G. Amoretti, Phys. Rev. Lett. **92**, 207205 (2004).
[43] N. Kirchner, J. van Slageren, B. Tsukerblat, O. Waldmann, and

M. Dressel, Phys. Rev. B **78**, 094426 (2008).
[44] C. M. Ramsey, E. Del Barco, S. Hill, S. J. Shah, C. C. Beedle, and D. N. Hendrickson, Nat. Phys. **4**, 277 (2008).
[45] C.-I. Yang, W. Wernsdorfer, G.-H. Lee, and H.-L. Tsai, J. Am. Chem. Soc. **129**, 456 (2007).
[46] M. Soler, W. Wernsdorfer, Z. Sun, J. Huffman, D. Hendrickson, and G. Christou, Chem. Commun. **2003**, 2672.
[47] S. Carretta, P. Santini, G. Amoretti, M. Affronte, A. Candini, A. Ghirri, I. S. Tidmarsh, R. H. Laye, R. Shaw, and E. J. L. McInnes, Phys. Rev. Lett. **97**, 207201 (2006).
[48] S. Piligkos, J. Bendix, H. Weihe, C. J. Milios, and E. K. Brechin, Dalton Trans. **2008**, 2277.
[49] S. Datta, E. Bolin, R. Inglis, C. J. Milios, E. K. Brechin, and S. Hill, Polyhedron **28**, 1788 (2009).